

Effect of Bubble/Droplet Morphology and Slippage on Attachment Induction Time in Deoiling Flotation Process

Mona Eftekhardakhah and Seyed Hassan Hashemabadi*

Computational Fluid Dynamics (CFD) Research Laboratory, School of Chemical Engineering, Iran University of Science and Technology, Tehran, Iran

(Received 7 May 2012, Accepted 12 March 2013)

Abstract

A modified model has been analytically developed to describe the induction time of an elliptic air bubble in contact with an elliptic hydrophobic oil droplet. The role of hydrophobicity was revealed in the slippage of liquid over the surfaces of bubble and droplet. In this condition, the analytical relationships for pressure distribution and consequently hydrodynamic resistance force through the water film have been reported. The obtaining results were compared with the previous models and different orientations of approaching bubble and droplet have been investigated. It was found that the induction time is very sensitive to the orientation of bubble and droplet in collision. On the other hand, the role of slippage can be shown by the decrease in pressure and hydrodynamic resistance force in liquid film and also in induction time, in comparison with the case of drainage of a film confined between two particles under no-slip boundary conditions on their surfaces.

Keywords: Analytical solution, Induction time, Oily wastewater, Particle morphology, Slippage

Introduction

Drop and bubble coalescence processes are an essential features of a great number of industrial and environmental systems such as de-oiling flotation [1], aerators, gas-liquid-liquid three phase reactors and so on. Oily wastewater processing can be done by gas flotation. This process is a gravitational separation technique in which small gas bubbles are injected into a water phase containing immiscible oil droplets, so the bubbles attach themselves to the oil droplets. In this way, the oil becomes lighter because of the increasing the density difference between the oil agglomerate and water, in consequence, the oil droplets rise faster and a shorter residence time is achieved in the separation unit. Finally, oil droplets form a foam layer on the surface of the wastewater which is skimmed off [2]. Bubble and droplet coalescence is complexly dependent on hydrodynamic and thermodynamic forces. The main sub-processes in this process are [3]:

- Increasing the oil droplet size by de-emulsification;
- Approach of oil drops and gas bubbles;
- Drainage and rupture of the confined liquid film;

- Attachment of gas bubbles to the oil as a result of spreading of oil drops over the gas bubbles.

The most critical stage between these sub-processes is the attachment of oil droplets to gas bubbles. This stage, itself involves the thinning and rupture of the liquid film between the oil droplet and gas bubble. The attachment process can be quantified by an important concept which is called induction time. Induction time is defined as the minimum time required for the thinning of the intervening film between bubble and droplet to a critical thickness and rupture spontaneously to form stable two-phase attachment in a mixture [4]. Induction time has a key role in bubble and droplet attachment because the efficiency of the process is diversely related to the induction time. According to the literature, the induction time can be defined as follows [5]:

$$t_{\text{ind}} = t_{\text{dr}} + t_r + t_e \quad (1)$$

Where t_{dr} is the drainage time of liquid film from an initial thickness (h_0) to a critical thickness (h_c), t_r is the time for the film rupture to form a nucleic hole; and t_e is

the time for expansion of the nucleic hole to a minimum radius at which the attachment can occur.

There are a lot of theoretical studies on film thinning and rupturing which represents that the induction time is a function of different parameters such as particle and bubble size [6 and 7]. Yoon and Yordan [8] and Ye et al. [9] showed that there is a logarithmic relationship between the induction time and particle size. Hewitt et al. [10] carried out single-bubble flotation tests and represented that estimated induction time decreased with decreasing bubble size. Schulze [11] developed an induction time model based on the Reynolds equation for the rate of squeezing a liquid film between two plane-parallel discs. In this model, liquid drainage time (t_{dr}) was assumed to be the induction time and two other terms (t_r and t_e) in Eq. (1) were assumed to be negligible, i.e.

$$t_{ind} \approx t_{dr} = \frac{3\mu r_0^2}{16\Delta p} \left(\frac{1}{h_c^2} - \frac{1}{h_0^2} \right) \quad (2)$$

Where Δp is the net force of interaction per unit area of the liquid film. It is obvious that this model over-simplified the physical problem of approaching two particles because of the assumption of two plane discs. There are several models available to describe the drainage rate of liquid film between an air bubble and a solid surface which were developed with considering two interfaces of the liquid film as two parallel plates, therefore they seldom used to calculate the induction time in flotation systems. Ye et al. [9] established an induction time model based on the existing forces at bubble-particle interface. This model was included the diameter of the particle as one parameter. Li et al. [12] developed another induction time model to describe the effect of bubble and particle size on the induction time. The results of this model showed good agreement with the reported experimental data by Ye et al. [9]. Wang et al. [13] considered the effect of curvature of bubbles or particles surfaces

and established an induction time model based on theoretical analysis:

$$t_{ind} \approx t_{dr} = -\frac{6\pi\mu R_b^2}{\bar{F}_0} \left(1 + \frac{R_b}{R_p} \right)^{-2} \ln \left(\frac{h_c}{h_0} \right) \quad (3)$$

Where \bar{F}_0 is the average net driving force for the water film drainage and rupture over the distance from initial (h_0) to critical (h_c) film thickness. R_b and R_p are the air bubble and hydrophobic particle radius respectively. Eftekhardadkhan and Hashemabadi [14] studied influence of bubble and droplet shape and size on flotation induction time while drainage water film is subjected to no slip condition. Their results show the size and morphology of bubbles and droplets have considerable effects on induction time.

As it is shown, more of these models described the induction time in flotation systems which were used in the separation of solid particles from wastewater and they fail to consider the effect of deformation of bubbles and droplets in de-oiling flotation units under dynamic conditions. Moreover, it should be noted that the thin film is not bounded by parallel planes in poly-dispersed systems and when drops or bubbles approach each other, it forms a dimple [12]. There are a great number of studies in this regard [15 and 16]. Because of the non-linear nature of the equations describing dimple formation, the problem of drainage has been studied mainly numerically by different authors [17-19].

In this paper, some modifications are applied to the previous induction time models by considering the elliptic shape for an air bubble and a hydrophobic oil droplet. Moreover, the influence of slip boundary condition on the surface of bubbles and droplets on induction time investigated. One major assumption which is considered in modeling is that the film thickness between bubble and droplet is negligibly small compared with radius of surface curvature and also dimple formation is not consider in the modeling in order to obtain analytically an exact equation for induction time.

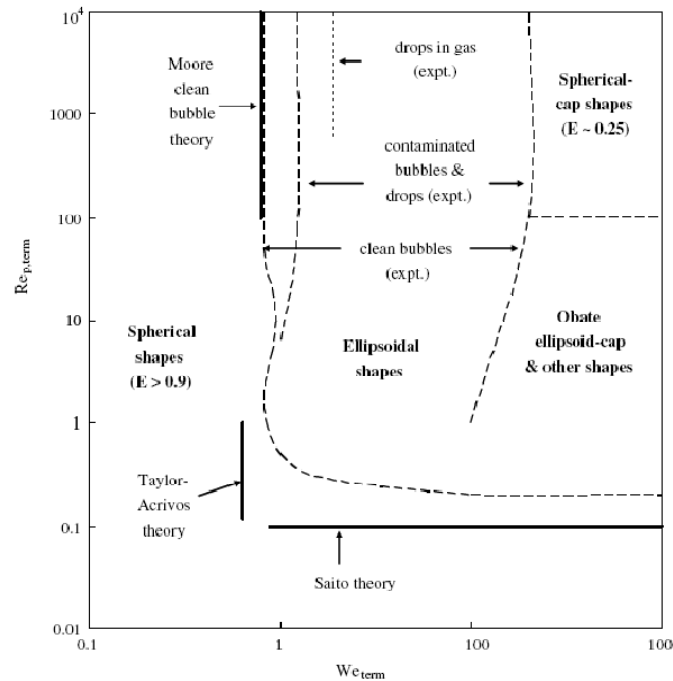


Figure 1: Shape of bubbles and drops as a function of Reynolds and Weber numbers [20].

Although this model is applicable under restricted conditions but it could explain qualitatively the effect of surface curvature of bubbles/drops, different approaching orientation and slip boundary condition on induction time that has not yet been reported.

Bubbles and droplets deformation

Dispersed droplets and bubbles can be deformed as a result of the interaction between surface tension and the fluid dynamic stresses on their surfaces. So, the morphology of the bubble or drop is not stable and changes due to the local stresses of the surrounding continuous phase. The surface tension forces will drive a free bubble or droplet toward a spherical shape, whereas dynamic forces are the effective sources of non-sphericity [20]. Moreover, these dynamic forces can be the reason of the pressure distribution on bubbles or drops surfaces. This pressure distribution can be presented by the viscosity ratio and the Reynolds number which control the recirculation and importance of viscosity, respectively. On the other hand, deformation is also related to the surface tension. Thus, Weber number, which is the

ratio of continuous phase stresses to surface tension stresses, shows influence of interfacial surface tension on deformation and it can be calculated by:

$$We = \frac{\rho_c w^2 d}{\sigma} \quad (4)$$

According to the work of Loth [20] the relationship between the bubbles or drops morphology and Reynolds and Weber number can be expressed as follow (at finite Re_p):

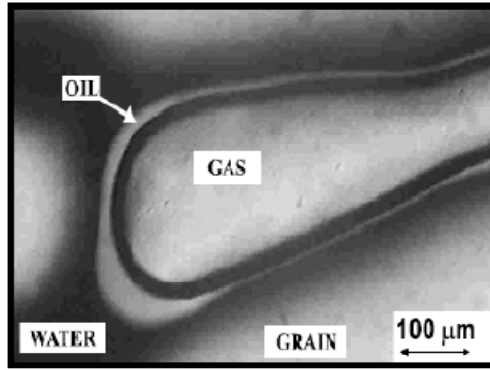
- $We \ll 1$ Particles rapidly tend to spherical geometry
- $We \sim 1$ Moderate deviation from a sphere can occur
- $We \gg 1$ Large deviation from a sphere can occur

The quantitative boundaries for terminal shapes for bubbles and droplets are shown in Figure 1.

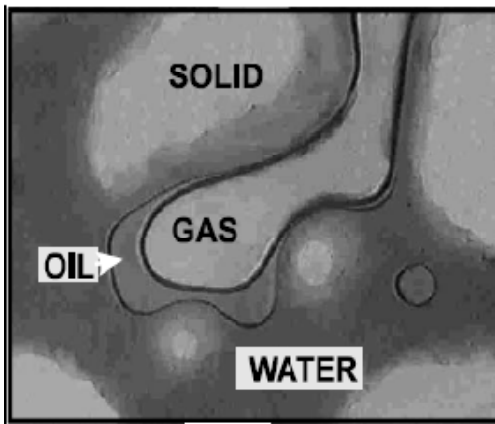
It is clear that the shape of bubbles or droplets is ellipsoidal in wide range of Re and We numbers. E is the ratio of the diameter along the axis of symmetry to the other diameter perpendicular to symmetry axis.

In another view, according to the images which were taken from real flotation

systems under dynamic condition, it can obviously be seen that the shape of bubbles and droplets are not spherical and their shapes are really close to ellipse as it is shown in Figure 2 [21]. So, the ellipsoidal shape for air bubble and oil droplet in de-oiling flotation process is reasonable.



(a)



(b)

Figure 2: (a) Magnification of gas-oil-water surface for spreading oil conditions, (b) Gas-oil-water configuration for spreading of oil [20].

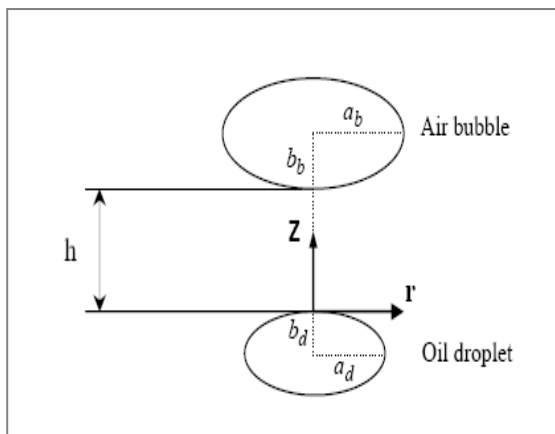


Figure 3: Schematic representation of elliptical air bubble and oil droplet

Mathematical modeling

The elliptic shape for bubbles and drops

Figure 3 shows the schematic representation of two ellipses as an air bubble and an oil droplet which were considered in the modeling.

The continuous phase is a Newtonian fluid. Two particles approach each other along the line which connects their centers. As shown in Figure 3, a cylindrical coordination system (z, r) can be defined such that the z -axis coincides with the connecting line and its origin is on the top of oil droplet. So, the plane $z=0$ which is tangent to the oil drop, can be expressed as follows:

$$z = -\frac{1}{2} \frac{b_d}{a_d^2} r^2 + O(r^4) \quad (5)$$

In a similar way, the surface of air bubble can be described as

$$z = h + \frac{1}{2} \frac{b_b}{a_b^2} r^2 + O(r^4) \quad (6)$$

Where h is the distance between the bubble and droplet. In order to simplify the equations, a modified system of coordinates (Z, r) is considered as follow:

$$Z = z + \frac{1}{2} \frac{b_d}{a_d^2} r^2 \quad (7)$$

So, in new translated coordinate the surfaces equation of oil drop is:

$$Z = O(r^4) = 0 \quad (8)$$

And air bubble surface profile is expressed as:

$$Z = h + \frac{1}{2} \alpha r^2 + O(r^4) = h + \frac{1}{2} \alpha r^2 = H \quad (9)$$

Where

$$\alpha = \frac{1}{b_b n_b^2} + \frac{1}{b_d n_d^2}, \quad n_b = \frac{a_b}{b_b}, \quad n_d = \frac{a_d}{b_d}$$

In new coordinate, the boundary conditions at oil droplet surface can be described as follows:

$$Z = 0, \quad v_z = 0, \quad v_r = 0 \quad (10)$$

At air bubble surface:

$$Z = H, \quad v_z = v_h, \quad v_r = 0 \quad (11)$$

Where v_h is the z -component of the fluid velocity at the surface very close to the

bubble. Because the magnification of h is negligibly small compared with the scale of bubble or droplet, it will lead to the equations of Reynolds approximation. In steady state for Newtonian fluid, the continuity and momentum equations are [22]:

$$\frac{1}{r} \frac{\partial}{\partial r} (rv_r) + \frac{\partial v_z}{\partial Z} = 0 \quad (12)$$

$$\rho \left(v_z \frac{\partial v_r}{\partial Z} + v_r \frac{\partial v_r}{\partial r} \right) = -\frac{\partial p}{\partial r} + \mu \left[\frac{\partial^2 v_r}{\partial Z^2} + \frac{1}{r} \frac{\partial}{\partial r} \left(r \frac{\partial v_r}{\partial r} \right) - \frac{v_r}{r^2} \right] \quad (13)$$

$$\rho \left(v_z \frac{\partial v_z}{\partial Z} + v_r \frac{\partial v_z}{\partial r} \right) = -\frac{\partial p}{\partial Z} + \mu \left[\frac{\partial^2 v_z}{\partial Z^2} + \frac{1}{r} \frac{\partial}{\partial r} \left(r \frac{\partial v_z}{\partial r} \right) \right] \quad (14)$$

All body forces are assumed negligible. Considering low Reynolds water film drainage, the motion equations (Eqs. 13 and 14) can be simplified to the following form:

$$\mu \left(\frac{\partial^2 v_r}{\partial Z^2} \right) = \frac{\partial p}{\partial r} \quad (15)$$

$$\frac{\partial p}{\partial Z} = 0 \quad (16)$$

The z -momentum diffusion terms in comparison with diffusion terms in r -coordinate direction are not considerable. The r -component of the fluid velocity is obtained by integrating Eq. (15) twice and considering boundary conditions, Eqs. (10) and (11):

$$v_r = \frac{1}{2\mu} \frac{dp}{dr} (Z^2 - ZH) \quad (17)$$

Now, integrating the continuity equation (Eq. 12), with taking into account the v_r , the z -component of the fluid velocity can be calculated:

$$v_z = -\frac{1}{2\mu r} \frac{\partial}{\partial r} \left[r \frac{dp}{dr} \left(\frac{Z^3}{3} - \frac{Z^2 H}{2} \right) \right] \quad (18)$$

Considering the symmetry of pressure distribution $\left(\frac{dp}{dr} \Big|_{r=0} = 0 \right)$, the differential equation for the fluid pressure very close to the bubble surface ($Z=H$), can be obtained by integrating Eq. (18)

$$\frac{dp}{dr} = 6\mu v_h \frac{r}{H^3} = 6\mu v_h r \left(h + \frac{1}{2} \alpha r^2 \right)^{-3} \quad (19)$$

The pressure distribution close to the bubble surface is calculated by integrating Eq. (19) and taking into account that $p=0$ while $r \rightarrow \infty$

$$p = -\frac{3\mu v_h}{\alpha} \left(h + \frac{1}{2} \alpha r^2 \right)^{-2} \quad (20)$$

Now, the hydrodynamic resistance force acting on the bubble surface can be determined:

$$F_z = -\int_0^\infty \left(-p + 2\mu \frac{dv_z}{dz} \right) 2\pi r dr \quad (21)$$

The pressure term in Eq. (21) is much greater than the other term. So, the net driving force acting on the bubble surface for the film drainage (F_0) is equal to the fluid resistance force (F_z) but with opposite sign:

$$F_o = \frac{6\pi\mu v_h}{h\alpha^2} \quad (22)$$

This equation can be rearranged as follows:

$$v_h = -\frac{dh}{dt} = \frac{1}{6\pi\mu} \alpha^2 F_o h \quad (23)$$

Finally, the induction time can be obtained by integrating Eq. (23) from initial to critical thickness of water film:

$$t_{ind} \approx t_{dr} = -\frac{6\pi\mu}{\alpha^2} \int_{h_0}^{h_c} \frac{1}{F_o h} dh = -\frac{6\pi\mu}{F_o \alpha^2} \ln \left(\frac{h_c}{h_0} \right) \quad (24)$$

It should be noted here that this model is obtained by considering an average value for F_o during the drainage of the liquid film.

The Slip flow boundary condition

In this study, the influence of hydrophobicity of oil drop and air bubble on induction time is determined by applying the same slippage model which was used by Vinogradova [23]. This model links the slippage effect with a decrease in the viscosity of a boundary layer close to a hydrophobic surface. In such a model, the slip velocity (v_{slip}) on the surface is proportional to the bulk shear stress:

$$v_{slip} = \lambda \frac{\partial v_{bulk}}{\partial z} \quad (25)$$

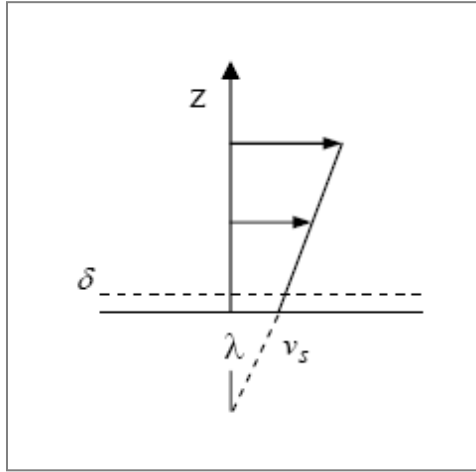


Figure 4: Schematic characterization of slip length [23].

Figure 4 describes the parameters of the applied slip model. The order of magnitude λ can be estimated as [23]:

$$\lambda = \delta \left(\frac{\mu_{bulk}}{\mu_{slip}} - 1 \right) \quad (26)$$

According to this slippage theory, λ can vary between two limited values. While the slip length approaches to zero, slip velocity is equal to zero which corresponds to the no-slip condition at the liquid/solid interface and the other limit is when λ approaches infinity normal gradient of slip velocity (v_{slip}) equals zero which corresponds to the conventional condition for a liquid/gas interface. So, the hydrodynamic equations (Eqs. 12, 15 and 16) retained without any change, but the no-slip boundary conditions replaced by a slippage law i.e.

$$Z=0, \quad v_r = \lambda \frac{\partial v_r}{\partial Z} \quad (27)$$

$$Z=H, \quad v_r = -\lambda(k+1) \frac{\partial v_r}{\partial Z} \quad (28)$$

Where k is a parameter which represents the hydrophobicity condition of the two phase interface. Vinogradova [23] considered three limiting cases for k . The hydrophobicity factor (k) can be minus one, zero and infinity which present interacting a hydrophobic particle with a hydrophilic one, hydrophobic one and with a bubble, respectively.

Therefore, following the same procedure as section 3.1, the components of fluid velocity can be obtained as follows:

$$v_r = \frac{1}{2\mu} \frac{\partial p}{\partial r} \left[\begin{array}{l} Z^2 - \frac{ZH(H+2\lambda(1+k))}{H+\lambda(2+k)} \\ \frac{\lambda H(H+2\lambda(1+k))}{H+\lambda(2+k)} \end{array} \right] \quad (29)$$

$$v_z = -\frac{1}{2\mu} \frac{1}{r} \frac{\partial}{\partial r} \left[r \frac{\partial p}{\partial r} \left(\begin{array}{l} \frac{Z^3}{3} - \frac{Z^2 H(H+2\lambda(1+k))}{2(H+\lambda(2+k))} \\ - \frac{Z\lambda H(H+2\lambda(1+k))}{H+\lambda(2+k)} \end{array} \right) \right] \quad (30)$$

Now, considering the region very close to the bubble surface ($Z=H, v_z=v_h$), above equation can be rewritten as:

$$\frac{d}{dr} \left(X^{-1} r \frac{dp}{dr} \right) = 2\mu v_h r \quad (31)$$

Where

$$X = \frac{6(A+H)}{-H^2(H+B)(H+C)}, \quad (32)$$

$$A = \lambda(2+k)$$

$$B = 2\lambda(2+k + \sqrt{1+k+k^2})$$

$$C = 2\lambda(2+k - \sqrt{1+k+k^2})$$

Integrating Eq. (31) twice and taking into account $dp/dr = 0$ at $r=0$ (due to symmetry of pressure distribution) and $p=0$ while radius approaches to infinity, the expression for pressure distribution can be derived:

$$p = \frac{3\mu v_h}{\alpha H^2} p^* \quad (33)$$

Where dimensionless function p^* is:

$$p^* = \frac{2AH}{BC} + \frac{2H^2}{(C-B)} \left[\begin{array}{l} \frac{(B-A)}{B^2} \ln \left(1 + \frac{B}{H} \right) \\ + \frac{(A-C)}{C^2} \ln \left(1 + \frac{C}{H} \right) \end{array} \right] \quad (34)$$

Now, with using Eq. (21) the net driving force acting on the bubble surface for the film drainage can be calculated as:

$$F_0 = \frac{6\pi\mu v_h}{\alpha^2 h} F^* \quad (35)$$

Where

$$F^* = \frac{2Ah}{BC} + \frac{2h}{(C-B)} \left[\frac{(B-A)(B+h)}{B^2} \ln\left(1 + \frac{B}{h}\right) + \frac{(A-C)(C+h)}{C^2} \ln\left(1 + \frac{C}{h}\right) \right] \quad (36)$$

Rearrangement of Eq. (35) leads to:

$$v_h = -\frac{dh}{dt} = \frac{F_o h}{6\pi\mu F^*} \alpha^2 \quad (37)$$

Finally, induction time can be calculated as follows:

$$t_{ind} \approx t_{dr} = \frac{6\pi\mu}{\alpha^2} \int_{h_0}^{h_c} \frac{F^*}{F_o h} dh = \frac{6\pi\mu}{F_o \alpha^2} t^* \quad (38)$$

Where

$$t^* = -\ln\left(\frac{h_c}{h_0}\right) + \beta \quad (39)$$

$$\beta = \frac{A}{BC} (h_c - h_0) + \frac{(B-A)}{(C-B)B^2} \left[(h_c + B)^2 \ln\left(1 + \frac{B}{h_c}\right) - (h_0 + B)^2 \ln\left(1 + \frac{B}{h_0}\right) \right] + \frac{(A-C)}{(C-B)C^2} \left[(h_c + C)^2 \ln\left(1 + \frac{C}{h_c}\right) - (h_0 + C)^2 \ln\left(1 + \frac{C}{h_0}\right) \right]$$

Where β is a correction factor for calculation of induction time in the presence of slip boundary condition on bubble and droplet surfaces, while two phase interface is subjected to no slip condition, β is equal to zero.

Results and discussion

Pressure distribution in water film

Figure 5 compares the pressure distribution in intervening film at $r=0$, for approaching two particles with ellipse and sphere shapes under slip and no-slip conditions.

It can clearly be seen that the amount of pressure in liquid film between bubble and drop under slip condition is less than while the film is subjected to no-slip condition for both ellipse and sphere shapes. This means that the role of slippage can be revealed by the decrease in pressure in comparison with the case of drainage of a film confined between two particles under no-slip boundary conditions on their surfaces; these results have a good agreement with the reported results by Vinogradova [23].

Moreover, deformation of particles from sphere to ellipse shape under both slip and non-slip conditions increases the amount of pressure in water film.

When the ellipse shape is considered for bubble and drop in the modeling, there are many orientations for approaching the air bubble and oil droplet. Four different orientations of elliptic bubble and droplet (**A**: $n_b \& n_d > 1$, **B**: $n_b \& n_d < 1$, **C**: $n_b > 1 \& n_d < 1$ and **D**: $n_b < 1 \& n_d > 1$) have been discussed here. The influence of different approaching conditions on pressure distribution can be determined by Eq. (21).

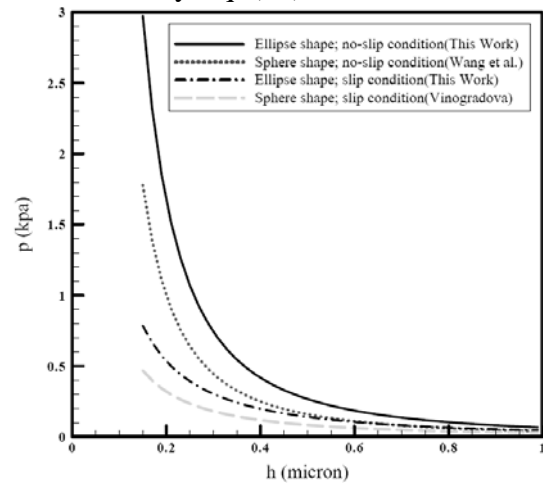


Figure 5: Comparison of pressure distribution in water film for different shapes (sphere and ellipse with $n_b = 2$; $n_d = 1.5$) and interface boundary conditions.

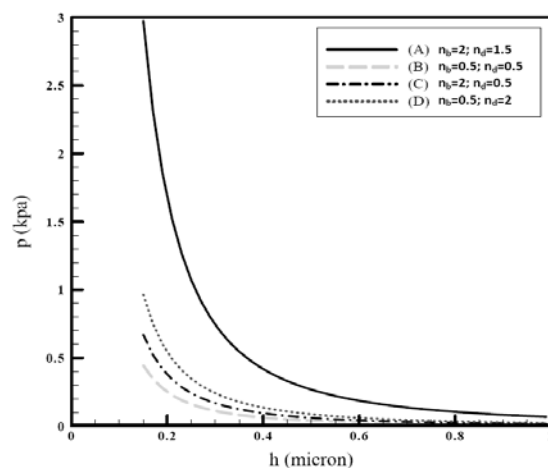


Figure 6: The effect of different approaching conditions on pressure distribution when bubble and droplet are elliptic.

As it is shown in Figure 6, the maximum pressure can be obtained when the bubble

and the droplet approach each other according to position (A) and minimum pressure is achieved for position (B).

Hydrodynamic resistance force in water film

Figure 7 illustrates the hydrodynamic resistance force distribution as a function of h in intervening film for approaching two particles with different shapes and different boundary conditions.

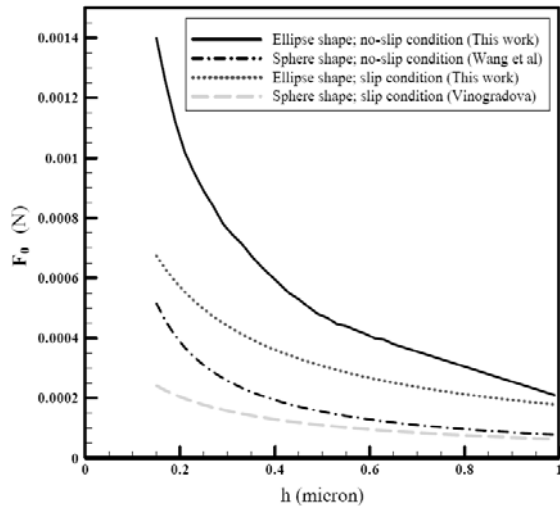


Figure 7: Comparison of hydrodynamic force on water film for different shapes (sphere and ellipse with $n_b = 2$; $n_d = 1.5$) and interface boundary conditions.

It can obviously be seen that the hydrodynamic force under slip condition decreases compared with the same results under no-slip condition. Therefore, the water drainage is occurred faster in the presence of slip boundary condition on bubble and drop surfaces. On the other hand, if gas bubbles and oil drops deform under dynamic conditions during drainage process and their shapes become elliptic, it can be lead to an increase in the hydrodynamic resistance force under both slip and no-slip conditions. Consequently, it can be concluded that the most amount of resistance against drainage can be obtained when bubbles and drops are elliptic under no-slip condition on their surfaces. The effect of different approaching conditions when bubble and drop are elliptic on hydrodynamic resistance force is presented in Figure 8. There is a significant difference

between the amounts of resistance force in position (A) in comparison with other approaching positions for air bubble and oil droplet. Therefore, in this form of approaching, the drainage process is slower than the others. It is clear that the behavior of pressure and hydrodynamic force in intervening liquid film between bubble and drop are very similar.

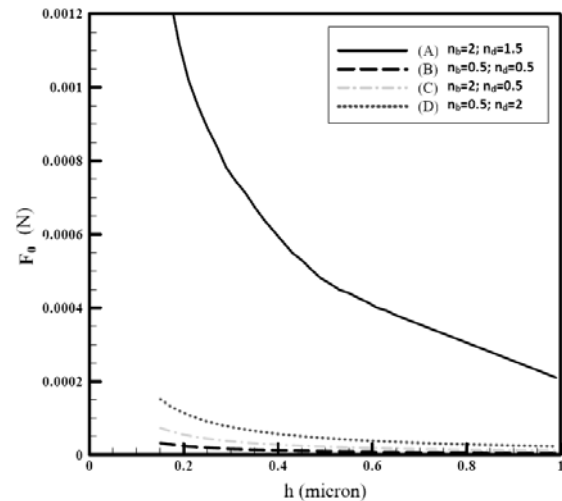


Figure 8: The influence of different approaching conditions on hydrodynamic resistance force when bubble and droplet are elliptic.

Induction time

The Influence of shape and boundary conditions

The influence of bubble size on the induction time for an air bubble in contact with oil droplet with different aspect ratio under slip and no slip conditions are shown in Figure 9. The results indicate that the induction time increases with promotion the bubble size for all cases. As it is mentioned before, the separation efficiency of flotation process decreases with increasing the induction time. So, in order to achieve higher separation efficiencies, producing fine bubbles is necessary. Moreover, as it is mentioned in previous sections, when bubble and droplet deform under dynamic conditions in flotation chamber and their shapes become elliptic, the pressure and hydrodynamic resistance force in intervening liquid film increase in comparison with when particles have

spherical shapes. Consequently, in this situation there is more resistance against drainage and the drainage process is very slow. Figure 9 illustrates this fact and it is clear that induction time for approaching two elliptical bubble and drop is more than for two sphere shapes particles. On the other hand, it seems that slippage is a factor which can overcome the hydrodynamic resistance force and help the liquid film drain faster. Therefore, under slip condition, induction time is less than that of similar case under no-slip condition.

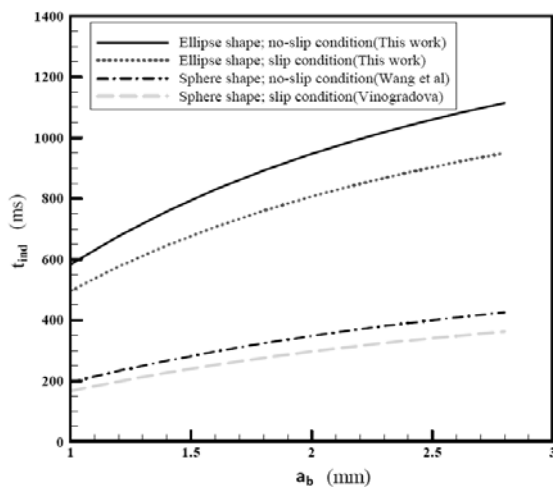


Figure 9: The induction time of elliptic air bubble and oil droplet with $n_b = 2$; $n_d = 1.5$ as a function of bubble size.

Influence of bubble and droplet orientation

The calculated amount of induction time as a function of bubble size for various approaching positions of bubble and drop are compared in Figure 10. It can clearly be seen that the higher induction time is calculated when bubble and drop approach each other according to position (A) which there is the most resistance (hydrodynamic force) against drainage, and induction time increases with increasing the n_b for a given oil droplet size. Furthermore, the less induction time is obtained for position (B), and in this case the flotation process has highest separation efficiency. With these theoretical results, the question is, how can we deform and impinge the bubbles and droplets into the flotation unit (according to

discussion in section 2) in order to achieving the higher efficiency in this process? It seems, this idea needs more investigation.

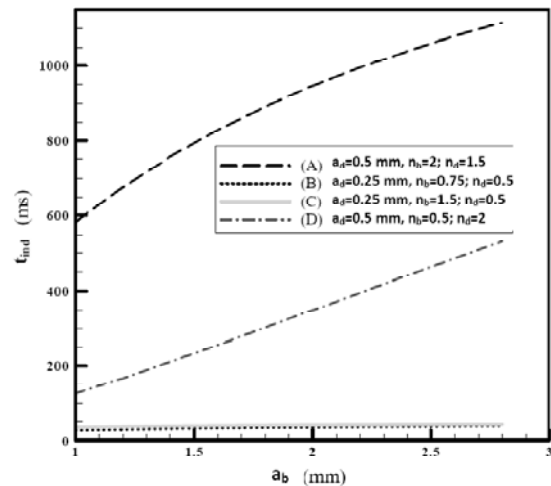


Figure 10: The effect of various approaching positions on induction time when bubble and droplet are elliptic.

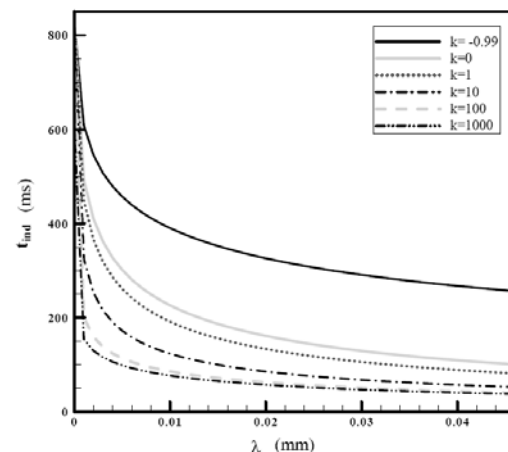


Figure 11: The influence of slippage parameters on induction time when bubble and droplet are elliptic with $n_b = 2$; $n_d = 1.5$.

Influence of slippage flow parameters

Figure 11 shows influence of slippage length (λ), and hydrophobicity factor k , on induction time. It can obviously be concluded that induction time decreases with increasing the slip length (λ), therefore the required time for drainage of a liquid film between two particles with solid surfaces is more than the bubbles and droplets. Moreover, the induction time decreases with increasing k from -0.99 to 1000 .

Therefore, the induction time for collision of a hydrophobic particle with a hydrophilic one is more than that of two hydrophobic particles and this is also more than the induction time for approaching a hydrophobic particle with a bubble.

Conclusion

Based on analytical solution of motion equation for film drainage between a bubble and a droplet under specific boundary conditions, a modified model has been developed to describe the induction time of an air bubble attaching to an oil droplet. The obtaining results were compared with previous works. The ellipse shape for bubble and drop due to presence of dynamic conditions in flotation chamber is considered in this study. This lead to an increase in the pressure and hydrodynamic resistance force in intervening liquid film between two particles and also in induction time, when is compared with the reported results of other researchers. Moreover, the effect of four different possible approaching positions of a bubble and a droplet ($n_b \& n_d > 1$, $n_b \& n_d < 1$, $n_b > 1 \& n_d < 1$ and $n_b < 1 \& n_d > 1$) have been studied. The attachment of air bubble and oil droplet has the maximum and minimum induction time while $n_b \& n_d > 1$ and $n_b \& n_d < 1$, respectively. Furthermore, the influence of presence of slip boundary condition on bubble and drop surfaces has been discussed. The results show that the role of slippage can be revealed by the decrease in pressure and hydrodynamic resistance force in liquid film and also in induction time in comparison with the case of drainage of a film confined between two particles under no-slip boundary conditions on their surfaces. As an overall conclusion, the most induction time was achieved when air bubble and oil droplet aspect ratio are greater than one in collision and their surfaces are subjected to no-slip boundary conditions. So, in this case flotation process has the lowest separation efficiency.

Nomenclature

A	Ellipse radius in r-direction
b	Ellipse radius in z-direction
d	Particle diameter
E	Dimensionless Symmetry parameter
F_0	Net driving force for drainage
F_z	Hydrodynamic resistance force acting on bubble surface
h	Separation distance between bubble and droplet (water film thickness)
H	Defined by Eq. (10)
k	Hydrophobicity factor
n	Aspect Ratio
p	Pressure
Δp	Net force of interaction per unit area of the liquid film
r	Radius of liquid film
R	Bubble or Particle radius
Re	Reynolds number
t	Time
v	Velocity
w	Relative Velocity of bubbles or drops
We	Weber number

Greeks

α	Defined by Eq. (10)
δ	Boundary layer thickness
λ	Slip length
μ	Viscosity
ρ	Density
σ	Surface tension

Subscript

0	Initial
b	Bubble
c	Critical
d	Droplet
dr	Drainage
e	Expansion
ind	Induction time
r	Rupture

Superscript

-	Average
---	---------

References:

- 1- Abid, S. and Chesters, A.K. (1993). "The drainage and rupture of partially mobile films between colliding drops at constant approach velocity." *Int. J. Multiphase Flow*, Vol. 20, pp. 613-629.
 - 2- Moosai, R. and Dawe, R.A. (2002). "Oily wastewater cleanup by gas flotation." *West Indian J. Eng.*, Vol. 25, pp. 25-41.
 - 3- Moosai, R. and Dawe, R.A. (2003). "Gas attachment of oil droplets for gas flotation for oily wastewater cleanup." *Separation and Purification Technol.*, Vol. 33, pp. 303-314.
 - 4- Gu, G., Sanders, R.S., Nandakumar, K., Xu, Z. and Masliyah, J.H. (2004). "A novel experimental technique to study single bubble-bitumen attachment in flotation." *Int. J. Mineral Processing*, Vol. 74, pp.15-29.
 - 5- Nguyen, A.V., Schulze, H.J. and Ralston, J. (1997). "Elementary steps in particle-bubble attachment." *Int. J. Mineral Processing*, Vol. 51, pp. 183-195.
 - 6- Taylor, G.I. and Michael, D.H. (1973). "On making holes in a sheet of fluid." *J. Fluid Mechanics*, Vol. 58, pp. 625-639.
 - 7- Prokhorov, A.V. and Derjaguin, B.V. (1994). "On the generalized theory of bi-layer film rupture." *Progress in Surface Science*, Vol. 45, pp. 29-39.
 - 8- Yoon, R. and Jordan, J.L. (1991). "Induction time measurements for the quartz-amine flotation system." *J. Colloid Interface Sci.*, Vol. 141, No. 2, pp.374-383.
 - 9- Ye, Y., Miller, J.D. and Khandrika, S.M. (1989). "Induction time measurements at a particle bed." *Int. J. Mineral Processing*, Vol. 25, pp. 221-240.
 - 10- Hewitt, D., Fornasiero and Ralston, J. (1995). "Bubble-particle attachment." *J. Chemical Society, Faraday Transactions*, Vol. 91, No. 13, pp. 1997-2001.
 - 11- Schulze H.J. (1984). "Physico-chemical elementary process in flotation." *Hydrometallurgy*, Vol. 12, pp. 275.
 - 12- Li, D., Fitzpatrick, J.A. and Slattery, J.C. (1990). "Rate of collection of particles by flotation." *Ind. Eng. Chem. Res.*, Vol. 29, No. 6, pp. 955-967.
 - 13- Wang, W., Zhou, Z., Nandakumar, K., Masliyah J.H. and Xu Z. (2005). "An induction time model for attachment of an air bubble to a hydrophobic sphere in aqueous solutions." *Mineral Processing*, Vol. 75, pp. 69-82.
 - 14- Eftekhardakhah, M. and Hashemabadi, S.H. (2008). "Influence of bubble and droplet shape and size on flotation time." Proc. of 12th Iranian Chemical Engineering Congress.
 - 15- Hodgison, T.D. and Woods, S.M. (1973). "The effect of applied force on drainage of the film between a liquid drop and horizontal surface." *AIChE J.*, Vol. 19, pp. 810-817.
-

- 16-Burrill, K.A. and Woods, D.R. (1973). "Film shapes for deformable drops at liquid-liquid interfaces II, The mechanisms of film drainage." *J. Colloid Interface Sci.*, Vol. 42, No. 1, pp. 15-34.
- 17-Malhotra, A.K. and Wasan, D.T., (1987). "Effect of film size on drainage of foam and emulsion films." *AIChE J.*, Vol. 33, No. 9, pp. 1533-1541.
- 18-Joye, J.L., Miller, C.A. and Hirasaki, G.J. (1992). "Dimple formation and behavior during axisymmetric foam film drainage." *Langmuir* 8, 3082.
- 19-Tsekov, R. and Ruckenstein, E. (1994). "Dimple formation and its effect on the rate of drainage in thin liquid films." *Colloids Surfaces*, Vol. 82, pp. 255-261.
- 20- Loth, E. (2008). "Quasi steady shape and drag of deformable bubbles and drops." *Int. J. Multiphase Flow*, Vol. 34, pp. 523-546.
- 21-Grattoni C., Moosai R. and Dawe R.A. (2003). "Photographic observations showing spreading and non-spreading of oil on gas bubbles of relevance to gas flotation for oily wastewater cleanup." *Colloids Surfaces*, Vol. 214, pp. 151-155.
- 22- Bird, R.B., Stewart, W.E. and Lightfoot, E.N. (2002). "Transport Phenomena." 2nd Edition, John Wiley & Sons Inc., New York.
- 23-Vinogradova, O.I. (1995). "Drainage of a thin liquid film confined between hydrophobic surfaces." *Langmuir*, Vol. 11, pp. 2213-2220.
-